

On local and global aspects of the 1:4 resonance in the conservative cubic Hénon maps.

M. Gonchenko¹, S.V. Gonchenko², I. Ovsyannikov^{2,3} and A. Vieiro¹

¹ Departament de Matemàtiques i Informàtica, Universitat de Barcelona, Spain

² N.I. Lobachevsky Nizhny Novgorod University, Russia

³ Fachbereich Mathematik und Informatik, Universität Bremen, Germany

gonchenko@ub.edu, gonchenko@pochta.ru, ivan.i.ovsyannikov@gmail.com, vieiro@maia.ub.es

Abstract

We study the 1:4 resonance for the conservative cubic Hénon maps \mathbf{C}_\pm with positive and negative cubic term. These maps show up different bifurcation structures both for fixed points with eigenvalues $\pm i$ and for 4-periodic orbits. While for \mathbf{C}_- the 1:4 resonance unfolding has the so-called Arnold degeneracy (the first Birkhoff twist coefficient equals (in absolute value) to the first resonant term coefficient), the map \mathbf{C}_+ has a different type of degeneracy because the resonant term can vanish. In the last case, non-symmetric points are created and destroyed at pitchfork bifurcations and, as a result of global bifurcations, the 1:4 resonant chain of islands rotates by $\pi/4$. For both maps several bifurcations are detected and illustrated.

Keywords: strong 1:4 resonance, cubic Hénon map, bifurcations, 4-periodic orbits.

Mathematical Subject Classification: 37G10, 37G20, 37G40, 37J10, 37J20.

1 Introduction

We study the 1:4 resonance problem for the conservative cubic Hénon maps

$$\mathbf{C}_- : \bar{x} = y, \quad \bar{y} = M_1 - x + M_2 y - y^3 \quad (1)$$

and

$$\mathbf{C}_+ : \bar{x} = y, \quad \bar{y} = M_1 - x + M_2 y + y^3, \quad (2)$$

where x, y are coordinates and M_1, M_2 are parameters.

For area-preserving maps, the basis of the 1:4 resonance phenomenon consists in a local bifurcation of a fixed (or periodic) point with eigenvalues $e^{\pm i\pi/2} = \pm i$. However, this can be only the simplest, standard part of the general picture of the resonance. As we show, the 1:4 resonance in the case of maps (1) and (2) can be nontrivial, i.e. it can include not only bifurcations of fixed points with eigenvalues $\pm i$ themselves (local aspects) but also a series of accompanying bifurcations (global aspects) of 4-periodic orbits which are initially born from the central fixed point with eigenvalues $\pm i$.

It is well-known that the strong resonances, i.e. the bifurcation phenomena connected with the existence of fixed (periodic) points with eigenvalues $e^{\pm 2\pi i/q}$ with $q = 1, 2, 3, 4$ (that is, the 1:1, 1:2, 1:3 and 1:4 resonances), play a very important role in the dynamics of area-preserving maps. Among them, the 1:4 resonance (with $q = 4$) is, as a rule, the most complicated and least studied. For example, the resonances with $q = 1, 2, 3$ are nondegenerate for the standard conservative Hénon map

$$\bar{x} = y, \quad \bar{y} = M - x - y^2. \quad (3)$$

Unlike this, the resonance 1:4 is degenerate here [Bir87, SV09].

The Birkhoff local normal form at the fixed point with multipliers $\pm i$, expressed in complex coordinates $z = x + iy$ and $z^* = x - iy$, can be written as follows

$$\bar{z} = iz + (B_{21}|z|^2 + B_{32}|z|^4)z + B_{03}(z^*)^3 + B_{50}z^5 + B_{14}z(z^*)^4 + O(|z|^7), \quad (4)$$

where, a priori, the coefficients B_{ij} are complex. The area-preserving property requires that (i) $\text{Im}(B_{21}) = 0$, (ii) $-3B_{03}^*B_{21} - 5iB_{50} + iB_{14}^* = 0$, and (iii) $3B_{21}^2 + 6\text{Im}(B_{32}) - 9|B_{03}|^2 = 0$. Moreover, rotating the complex coordinates one can consider B_{03} real. Condition (ii) implies in this case that $\text{Re}(B_{14}) = 5\text{Re}(B_{50})$. The main nondegeneracy conditions of the normal form (4) are as follows

$$B_{03} \neq 0 \text{ and } A = \left| \frac{B_{21}}{B_{03}} \right| \neq 1. \quad (5)$$

The simplest degeneracies occur when only one of the conditions in (5) does not hold.

The local bifurcations at the 1:4 resonance, in the general (not necessarily conservative) setting, were first studied by V. Arnold in the 70's, see [Arn88], for the flow normal form $\dot{z} = \varepsilon z + \tilde{A}z|z|^2 + (z^*)^3$, where \tilde{A} is a coefficient and ε is a small complex parameter.¹ He showed that the structure of such resonance essentially depends on the relation between $\text{Re } \tilde{A}$ and $\text{Im } \tilde{A}$ and he studied several cases, e.g. when $|\tilde{A}| < 1$ or $|\text{Re } \tilde{A}| > 1$. Numerous other cases (when $|\text{Re } \tilde{A}| < 1$ and $|\tilde{A}| > 1$) were studied in many papers, see e.g. [Kra94, Kuz95]. Concerning the conservative case, where $\text{Re } \tilde{A} \equiv 0$, the Arnold normal form can be represented as

$$\dot{z} = i\varepsilon z + ibz|z|^2 + i(z^*)^3, \quad (6)$$

where ε and $b = \text{Im}(\tilde{A})$ are real. This normal form is nondegenerate in the case $b \neq 1$ and its bifurcations are well-known, see Fig. 1. We see that cases $b < -1$, Fig. 1a, and $|b| < 1$, Fig. 1b, are very different. In particular, the equilibrium $z = 0$ is always stable in the first case, whereas, it can be unstable (a saddle with 8 separatrices, at $\varepsilon = 0$) in the second case.

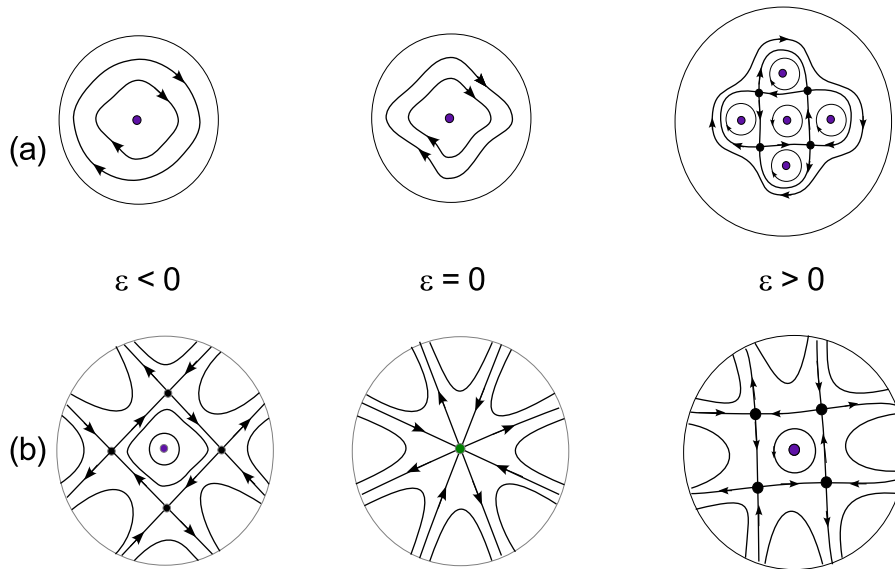


Figure 1: Bifurcations of zero equilibrium in the family (6) for $|b| \neq 1$ in the cases (a) $b < -1$, here only one equilibrium $z = 0$ (a nonlinear center) exists at $\varepsilon \leq 0$ and 8 equilibria appear surrounding $z = 0$ at $\varepsilon > 0$; and (b) $|b| < 1$, here 5 equilibria (4 saddles and the center $z = 0$) exist at $\varepsilon < 0$; at $\varepsilon = 0$ all these equilibria merge to the point $z = 0$ which becomes the nonhyperbolic saddle with 8 separatrices; at $\varepsilon > 0$ the point $z = 0$ becomes again a center and the 4 saddles appear to be rotated by $\pi/4$ with respect to the ones at $\varepsilon < 0$. Note that, in case $b > 1$, one needs to change both ε by $-\varepsilon$ and the time direction in the (a) row of the plot.

As it was shown in [Bir87, SV09], in the case of map (3), the degeneracy $A = 1$ (here $B_{21} = -B_{03}$) takes place. Note that the Hénon map (3) has a fixed point with eigenvalues $\pm i$ at $M = 0$. As it was shown in [Bir87], the family $\bar{x} = y, \quad \bar{y} = \varepsilon_1 - x - y^2 + \varepsilon_2 y^3$ can be considered as a two-parameter general unfolding for the study of

¹However, one can consider that ε varies inside the unit circle $|\varepsilon| = 1$ (as it was done e.g. in [AAIS86]) by rescaling $t = T/|\varepsilon|, z = Z|\varepsilon|$.

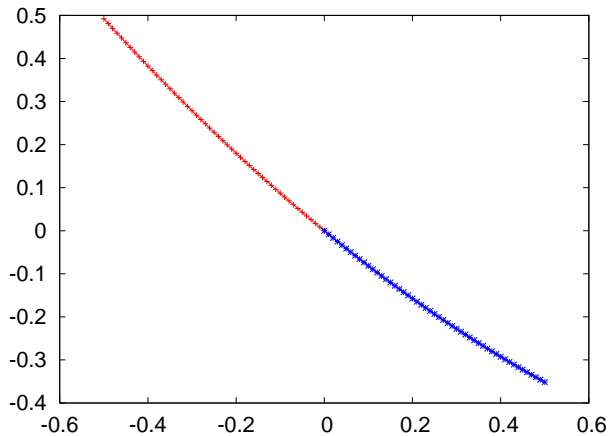


Figure 2: We represent the value of the Birkhoff twist coefficient Ω of \mathbf{C}_+ (for $M_2 < 0$) and of \mathbf{C}_- (for $M_2 > 0$) as a function of M_2 .

bifurcations of this point. This result is quite important, since such maps (conservative Hénon maps with small cubic term) appear naturally as rescaled first return maps near homoclinic orbits to saddle-focus equilibria of divergence-free three-dimensional flows [BS89] or near quadratic homoclinic tangencies of area-preserving maps [GG09, DGG15].²

In the present paper we show that degeneracy $A = 1$ can take place only in the case of cubic map (1) (here $B_{03} < 0$ always). This occurs for $M_1 = \pm 16/27$ and $M_2 = 1/3$. For those parameter values one has $B_{21} \neq 0$ and $B_{03} \neq 0$, see Section 3 for the concrete expressions of these coefficients as a function of M_2 . Then, according to [Bir87], case $A = 1$ is generic whenever the coefficient $\Omega = \text{Re}(B_{32} - B_{50} - B_{14})$ is non-zero, which guarantees a non-vanishing twist for the 4th power of the local normal form (4). We show in Fig. 2 the graph of Ω for \mathbf{C}_- and \mathbf{C}_+ as a function of M_2 . In particular, we see that $\Omega \approx -0.25$ when degeneracy $A = 1$ takes place for \mathbf{C}_- . A description of the local bifurcations in normal form (4) with $A = 1$, $\Omega \neq 0$ was also given in [Bir87]. However, we do not restrict ourselves only to the study of the local structure of this resonance – the analysis of the corresponding normal form is quite standard. We also study the global effect of this resonance on the dynamics of map (1) as a whole. To this end, we find (analytically and/or numerically) bifurcation curves relevant to describe the bifurcation diagrams related to both bifurcations of the fixed point with eigenvalues $\pm i$ as well as to accompanying bifurcations of saddle and elliptic 4-periodic orbits belonging to the corresponding resonant garland surrounding the fixed point. We collect the corresponding results in Section 3.

We also show that degeneracy $B_{03} = 0$ can take place only in the case of the cubic map (2), when $M_1 = \pm 20/27$ and $M_2 = -1/3$ (for this map $B_{21} \neq 0$ always). Moreover, for map \mathbf{C}_+ , the value of A is always greater than 1. As in the case of map (1), we study both the local and global aspects of this resonance, see Section 4.

As far as we know, this type of the conservative 1:4 resonance (with $B_{03} = 0$) has not been studied before,³ therefore we describe the main elements of the local bifurcations at such resonance in the Appendix B. In this case we assume $B_{14}^* = 5B_{50} \neq 0$. Note that the previous equality of the coefficients guarantees the Hamiltonian character of the corresponding flow normal form (see Eq.(9) in Section 2), while the nonvanishing of those coefficients is an additional nondegeneracy condition. In Fig. 3 we show the graphs of B_{14} and B_{50} , for the case of map (2), as a function of M_2 . In particular, when degeneracy $B_{03} = 0$ takes place in map (2) ($M_1 = \pm 20/27$, $M_2 = -1/3$), one has that $B_{14} \approx -5/64$.

We note that the cubic Hénon maps (1)-(2) have an important meaning for the theory of dynamical systems. For example, they appear as truncated normal forms of first return maps near cubic homoclinic tangencies. In Fig. 4 we illustrate the geometric idea how such maps can be obtained. Let a two-dimensional map f have a fixed saddle point O and a homoclinic orbit Γ at whose points the manifolds $W^u(O)$ and $W^s(O)$ have a cubic tangency. Let $M^+ \in W_{loc}^s$

² The main bifurcations of area-preserving maps with quadratic homoclinic tangencies were studied in [MR97, GG09, DGG15], and with cubic ones in [GGO17]. In all these papers, the main technical tool was the so-called rescaling method by which it was possible to represent the first return map in the form of a map being asymptotically close to the quadratic or to the cubic Hénon map.

³However, it was noted in [GLRT14, GT17] that such type resonances can provoke symmetry-breaking bifurcations (of pitchfork type) which, in the case of reversible maps, lead to the appearance of nonconservative periodic orbits (e.g. periodic sinks and sources).

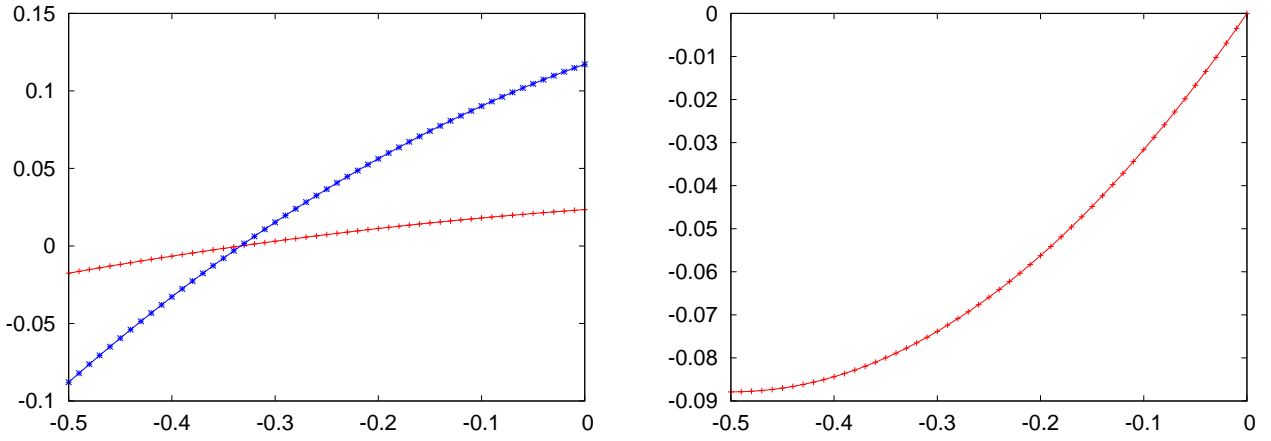


Figure 3: For map \mathbf{C}_+ , we represent in the left plot the values of $\text{Im}(B_{14})$ (in red) and of $5\text{Im}(B_{50})$ (in blue) as a function of M_2 . Both lines cross at 0 for the value $M_2 = -1/3$ where degeneracy $B_{03} = 0$ takes place. In the right plot we represent $\text{Re}(B_{14}) = 5\text{Re}(B_{50})$ as a function of M_2 for the same map.

and $M^- \in W_{loc}^u$ be a pair of points of Γ and σ_k be a small (horizontal) strip near M^+ . Under some number m of iterations of f the strip σ_k is mapped into a vertical strip $\tilde{\sigma}_k$ located near the point M^- . The (local) map from σ_k into $\tilde{\sigma}_k$ can be represented, for simplicity, as the linear map $\bar{x} = \lambda^m x, \bar{y} = \lambda^{-m} y$, where (x, y) are coordinates of points in σ_k and (\bar{x}, \bar{y}) are those in $\tilde{\sigma}_k$. Let q be an integer such that $f^q(M^-) = M^+$. Then, since the curve $f^q(W_{loc}^u)$ have a cubic tangency with W_{loc}^s at the point M^+ , the image $f^q(\tilde{\sigma}_k)$ of $\tilde{\sigma}_k$ will have the form of a cubic horseshoe. Thus, the geometry of the first return map $f^k : \sigma_k \rightarrow \sigma_k$, where $k = m + q$, is like the one of a cubic horseshoe map. If one rescales the initial coordinates (x, y) and the initial parameters μ_1 and μ_2 (that are the usual parameters that unfold the initial cubic homoclinic tangency between the curves $f^q(W_{loc}^u)$ and W_{loc}^s at the point M^+) in the appropriate way, then one can rewrite the map $f^k : \sigma_k \rightarrow \sigma_k$ in the form of a cubic Hénon maps with some terms that are asymptotically small as $k \rightarrow \infty$. Note that if $\lambda > 0$, then there are two different types of cubic homoclinic tangencies: the tangency “incoming from above”, see Fig. 4a, and the tangency “incoming from below”, see Fig. 4b. In the first case, the truncated rescaled map is map (1), while in the second case it is map (2). For more details, see [GGO17] for the area-preserving case and [GST96, GSV13] for the dissipative case.

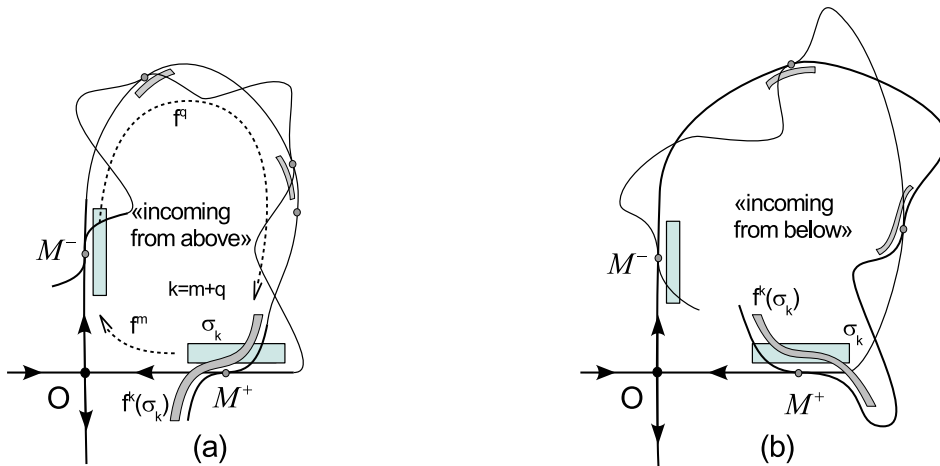


Figure 4: Two types of cubic homoclinic tangencies to a saddle fixed point with positive eigenvalues and geometry of the first return maps.

The main bifurcations of the dissipative cubic Hénon maps (when the absolute value of the Jacobian is less than 1)

were studied in [Gon85, GK88]. In the paper [DM00] some bifurcations of conservative maps (1) and (2) were studied. Note that one of the main goals of [DM00] was to describe the bifurcation structure of the 1:1, 1:2 and 1:3 strong resonances. The present work as well as the papers [Gon05, GGO17] are devoted mainly to the study of the local and global aspects of the 1:4 resonances, which complements the research of [DM00] on the dynamics and the bifurcations of the conservative cubic Hénon maps.

The paper is organised as follows. In Section 2 we review the 1:4 resonance for general area-preserving maps and comment about the degenerate cases. In Section 3 we consider map \mathbf{C}_- and describe the local and global aspects of the 1:4 resonance in this concrete case. The degeneracy $A = 1$ occurs here and we study its influence on the global bifurcation diagram. The same type of local and global bifurcation analysis is performed in Section 4 for the 1:4 resonance of the map \mathbf{C}_+ . We show that degeneracy $B_{03} = 0$ takes place in this case. As far as we know, this degeneracy has not been studied before, therefore we include the normal form analysis of this bifurcation in Appendix B. For both maps, some of the bifurcation curves have been explicitly obtained and their equations are derived in Appendix A. Finally, in Section 5 we comment on related topics where the results obtained in this paper could be relevant.

2 Local aspects of the 1:4 resonance in area-preserving maps.

The unfolding of the non-degenerate 1:4 resonance leads to the one-parameter family of area-preserving maps

$$\bar{z} = ie^{i\tilde{\beta}}z + B_{21}z^2z^* + B_{03}(z^*)^3 + O(|z|^5), \quad (7)$$

being $\tilde{\beta}$ a real parameter characterizing the deviation of the angle argument φ of the eigenvalues of the fixed point from $\pi/2$ ($\varphi = \tilde{\beta} + \pi/2$), the coefficients $B_{21} := B_{21}(\tilde{\beta})$ and $B_{03} := B_{03}(\tilde{\beta})$ are real and depend smoothly on $\tilde{\beta}$. If $B_{03} \neq 0$, the fourth iteration of map (7) can be locally embedded into the one-parameter family (6) of Hamiltonian flows, being $b(\tilde{\beta}) = B_{21}(\tilde{\beta})/B_{03}(\tilde{\beta})$ and $\varepsilon = 4\tilde{\beta}/B_{03}$. Local bifurcations of this Hamiltonian system are shown in Fig. 1.

As mentioned in the introduction, the 1:4 resonance is degenerate whether $A = |b(0)| = 1$ or $B_{03}(0) = 0$, see (5).

The case $A = 1$ appears in the bifurcation diagram of \mathbf{C}_- , see Section 3. The unfolding of this case leads to a two-parameter family of area-preserving maps. The fourth iteration of such a family is close-to-identity and can be approximated by the flow of the Hamiltonian system

$$\dot{z} = i\beta z + i(1 + \mu)z|z|^2 + iz^{*3} + i\tilde{B}_{32}|z|^4z + i\tilde{B}_{50}z^5 + i\tilde{B}_{14}|z|^2z^{*3} + O(|z|^7), \quad (8)$$

where $\beta = 4\tilde{\beta}/B_{03}$, μ is the parameter responsible for the deviation from $A = 1$. The coefficients \tilde{B}_{ij} are related to those in (4), see [Bir87, GG14, SV09]. Namely, one has

$$1 + \mu = \frac{B_{21}}{B_{03}} + \mathcal{O}(\beta), \quad \tilde{B}_{32} = \frac{\text{Re}(B_{32})}{B_{03}} + \mathcal{O}(\beta), \quad \tilde{B}_{50} = \frac{\text{Re}(B_{50})}{B_{03}} + \mathcal{O}(\beta), \quad \tilde{B}_{14} = \frac{\text{Re}(B_{14})}{B_{03}} + \mathcal{O}(\beta).$$

The vector field has zero divergence provided that $5\tilde{B}_{50} = \tilde{B}_{14}$.

The bifurcation diagram for (8), when considering (β, μ) in a small neighbourhood of the origin (case $A = 1$), is displayed in Fig. 5. There are three bifurcation curves L_1 , L_2 and L_3 dividing the (β, μ) -parameter plane into 3 domains. Curves $L_1 : \{\beta = 0, \mu > 0\}$ and $L_2 : \{\beta = 0, \mu < 0\}$ correspond to the passage from I to II and II to III, respectively, and reconstructions of nonzero saddle equilibria occur. Curve $L_3 : \{\mu = \sqrt{-\beta\Omega} + O(|\beta|)\}$ corresponds to a $\pi/2$ -equivariant parabolic bifurcation: 4 saddles and 4 elliptic equilibria appear when crossing from I to III. This bifurcation takes place far away from the origin of coordinates and it is a codimension one bifurcation for (8) since the flow is invariant under the rotation of angle $\pi/2$. Note that the origin is a non-degenerate conservative center for $\beta \neq 0$; it is a degenerate saddle with 8 separatrices for $(\beta, \mu) \in L_1$ and a degenerate conservative center for $(\beta, \mu) \in L_2$. The origin in the (β, μ) -plane, which corresponds to the case $A = 1$, is the endpoint of all the three bifurcation curves. Note that, in Fig. 5, we represent the bifurcation diagram for the case $\Omega < 0$ because for map \mathbf{C}_- , as we have computed, one has $\Omega \approx -0.25$, see Fig. 2.

The unfolding of case $B_{03} = 0$ reduces to the study of the Hamiltonian flow

$$\dot{z} = i\hat{\beta}z + i\hat{B}_{21}z|z|^2 + i\hat{\varepsilon}z^{*3} + i\hat{B}_{32}|z|^4z + i\hat{B}_{50}z^5 + i\hat{B}_{14}|z|^2z^{*3} + O(|z|^7), \quad (9)$$

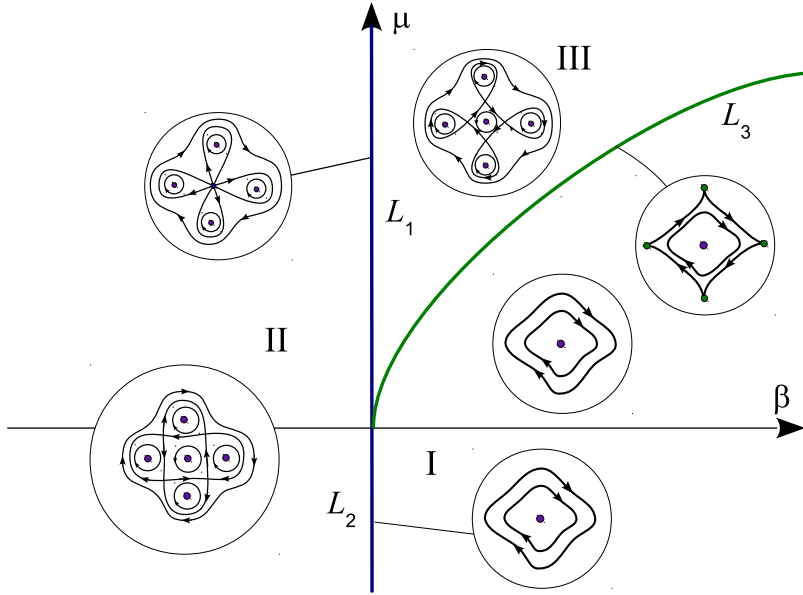


Figure 5: Main elements of bifurcation diagram in the case $A = 1$ (we assume $\Omega < 0$).

where $\hat{\beta} = 4\tilde{\beta}$ and ϵ are real parameters and $\hat{B}_{ij} = \text{Re}(B_{ij}) + \mathcal{O}(\hat{\beta})$ comparing with (4). This degeneracy appears only in the case of map \mathbf{C}_+ , see Section 4. The generic scenario happens whenever $B_{21} \neq 0$ and $\text{Re}(B_{50}) \neq 0$. The bifurcation diagram for (9), when considering $(\epsilon, \hat{\beta})$ in a small neighbourhood of the origin, is displayed in Fig. 6. The curve $L_2 : \{\hat{\beta} = 0\}$ corresponds to the 1:4 resonance of the fixed point (the equilibrium $z = 0$ of flow (9) has two zero eigenvalues). The curves $L^\pm : \{\hat{\beta} = \frac{\epsilon}{2\text{Re}(B_{50})} (B_{21} \pm \frac{\epsilon}{2}) + \mathcal{O}(\hat{\beta}\epsilon), \epsilon \text{Re}(B_{50}) < 0\}$ correspond to $\pi/2$ -equivariant pitchfork bifurcations related to the creation of 8 nonzero equilibria of the system (9) (4 of the equilibria correspond to a saddle 4-periodic orbit of the map while the other 4 equilibria correspond to an elliptic 4-periodic orbit of the map). The illustration in Fig. 6 corresponds to $\text{Re}(B_{50}) < 0$ and $B_{21} > 0$, as happens for the map \mathbf{C}_+ for $M_2 = -1/3$ when degeneracy $B_{03} = 0$ takes place (see Fig. 3 right and Section 4).

Note that normal forms (8) and (9) are Hamiltonian and reversible with respect to two linear involutions: involution $R : z \rightarrow z^*$ (in the real coordinates (x, y) , it corresponds to involution $(x, y) \rightarrow (x, -y)$) and involution $R^* : z \rightarrow iz^*$ (it corresponds to involution $(x, y) \rightarrow (y, x)$). Since flows (8) and (9) are $\pi/2$ -equivariant, two additional involutions also exist: $\tilde{R} : z \rightarrow -z^*$ (it corresponds to $(x, y) \rightarrow (-x, y)$) and $\tilde{R}^* : z \rightarrow -iz^*$ (it corresponds to the involution $(x, y) \rightarrow (-y, -x)$). The lines of fixed points of these involutions are the following: $\text{Fix}(R) = \{y = 0\}$; $\text{Fix}(\tilde{R}) = \{x = 0\}$; $\text{Fix}(R^*) = \{x = y\}$ and $\text{Fix}(\tilde{R}^*) = \{x = -y\}$.

Returning to the bifurcation diagram of Fig. 6, we see that at $(\hat{\beta}, \epsilon) \in \text{I}$ only one equilibrium exists (the trivial equilibrium $z = 0$ that is a center), while nontrivial equilibria (centers and saddles) appear in the other regions of the diagram. In regions II and IV there are 8 nontrivial equilibria while in region III there exist 16 nontrivial equilibria. In the case of regions II and IV, all nontrivial equilibria are symmetric, i.e. belong to the lines of fixed points of the involutions: in II two of the four centers belong to the axis $y = 0$ ($\text{Fix}(R)$) while the other two belong to $x = 0$ ($\text{Fix}(\tilde{R})$), and two of the four saddles belong to the bisectrix $x = y$ ($\text{Fix}(R^*)$) while the other two belong to $x = -y$ ($\text{Fix}(\tilde{R}^*)$). We see in region IV another disposition of these equilibria: the picture seems turned by an angle of $\pi/4$. Due to the strong reversibility properties of system (9), such simple rotation of the garland is impossible without bifurcations. The corresponding (providing such a rotation) symmetry breaking bifurcations, at the passage from domain II to domain IV, are schematically shown in Fig. 6. When passing from I to III_b, the centers undergo (supercritical) pitchfork bifurcations: they all become saddles and four pairs of nonsymmetric centers are born. The curve L_{hom} in domain III corresponds to a global $\pi/2$ -equivariant bifurcation of creation of heteroclinic connections between all 8 saddles.⁴ The passage through L_{hom} from III_b to III_a is related to reconstructions of the separatrices of the saddles. After this, at passage from III_a to IV, we observe a (subcritical) pitchfork bifurcation where asymmetric centers merge with symmetric saddles and the latter become centers.

⁴For the case of map \mathbf{C}_+ , a homoclinic zone should exist instead of the simple curve L_{hom} .

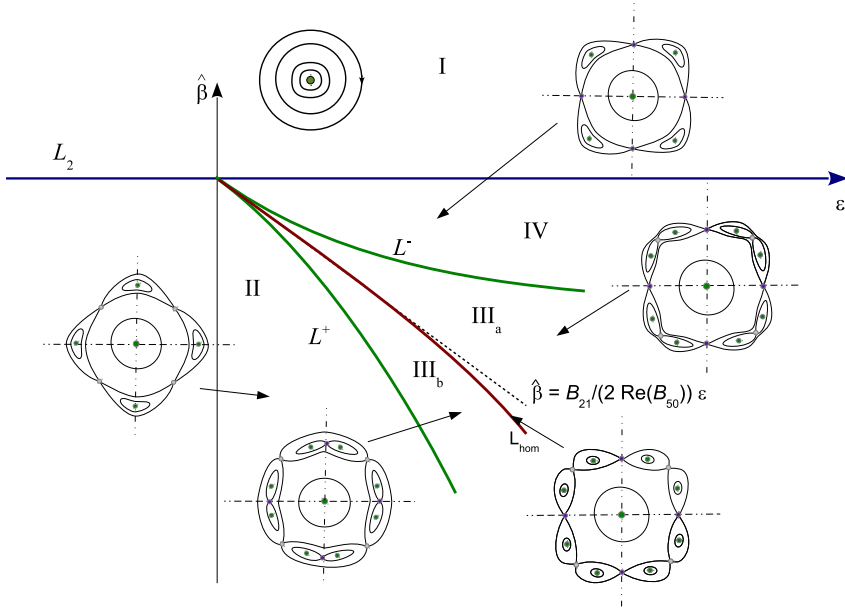


Figure 6: Main elements of the bifurcation diagram in case $B_{03} = 0$ (we assume $\operatorname{Re}(B_{50}) < 0$ and $B_{21} > 0$).

Some details of the analysis of normal form (9) are given in Appendix B ⁵. See Fig. 11 for the bifurcation scenario taking place for \mathbf{C}_+ when crossing the region III.

3 The 1:4 resonance in map \mathbf{C}_-

Consider map (1) with parameters (M_1, M_2) on the 1:4 resonance curve

$$L_{\pi/2}^- : M_1^2 = \frac{4}{27} M_2 (M_2 - 3)^2, \quad (10)$$

see Fig. 7. For $M_1 > 0$ (resp. $M_1 < 0$) map \mathbf{C}_- has $P_{\pi/2}^- = (-\sqrt{M_2/3}, -\sqrt{M_2/3})$ (resp. $P_{\pi/2}^+ = (\sqrt{M_2/3}, \sqrt{M_2/3})$) as a fixed point with eigenvalues $\pm i$. Note that $L_{\pi/2}^-$ has a self-intersection point $(M_1 = 0, M_2 = 3)$ where the map has two fixed points $(-1, -1)$ and $(1, 1)$ with eigenvalues $\pm i$ simultaneously.

The unfolding of normal form (7) at the fixed point $P_{\pi/2}^\pm$ (taking the suitable sign) has coefficients $8B_{21}(0) = -3 + 3M_2$, $8B_{03}(0) = -1 - 3M_2$, see [Gon05]. Since $M_2 \geq 0$ in curve $L_{\pi/2}^-$, we get $B_{03}(0) < 0$. Consequently, one has

$$A = \frac{|3 - 3M_2|}{1 + 3M_2},$$

and all the three cases $A > 1$, $A < 1$ (see Fig. 1), and $A = 1$ (see Fig. 5) take place for \mathbf{C}_- . The case $A = 1$ occurs at the points $P^+(M_1 = 16/27, M_2 = 1/3)$ and $P^-(M_1 = -16/27, M_2 = 1/3)$, both in curve $L_{\pi/2}^-$, see Fig. 7.

The bifurcation diagram of the 1:4 resonance in map \mathbf{C}_- is displayed in Fig. 7, where the bifurcation curves $L_{\pi/2}^-$, L_4^i and \tilde{L}_4^i , $i = 1, 2, 3, 4$, are shown in the (M_1, M_2) -parameter plane. The equation for $L_{\pi/2}^-$ is written in (10). The curves L_4^i , $i = 1, \dots, 4$, are the curves of parabolic 4-periodic orbits with double eigenvalue 1. The curves \tilde{L}_4^i , $i = 1, \dots, 4$, are the curves of parabolic 4-periodic orbits with double eigenvalue -1. Concretely:

- The curves $L_4^{1,2}$, whose equations are

$$L_4^{1,2} : 27M_1^2 = 4(1 + M_2)^3, \quad \text{where } M_2 > 1/3 \text{ and } M_1 > 0 \text{ for } L_4^1 \text{ while } M_1 < 0 \text{ for } L_4^2, \quad (11)$$

⁵ In Appendix B we denote $b_1 = \hat{\beta}$, $\mu = 2\epsilon$, $b_2 = 2\hat{B}_{21}$ and $B = 16\hat{B}_{50}$.

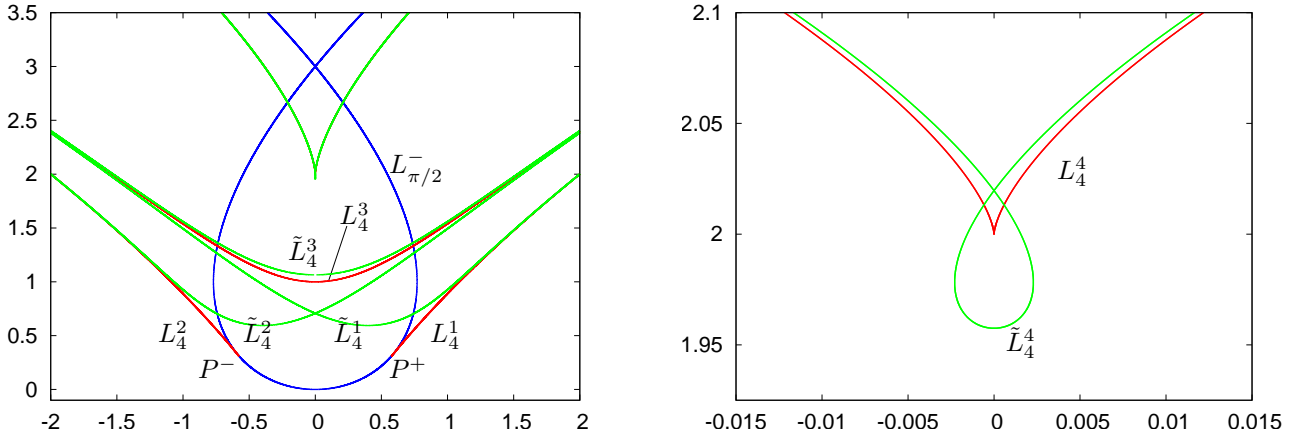


Figure 7: Left: Bifurcation curves for the map \mathbf{C}_- . Right: A zoom of the domain near $M_1 = 0, M_2 = 2$.

are quadratically tangent to the curve $L_{\pi/2}^-$ at the points P^\pm (case $A = 1$). When crossing $L_4^{1,2}$ from bottom to top two 4-periodic orbits are created as a result of a parabolic (elliptic-hyperbolic) bifurcation. Note that curves $L_4^{1,2}$ come from the L_3 curve in Fig. 5.

- The curve L_4^3 , given by

$$L_4^3 : 27M_1^2 = 4(2 + M_2)^2(M_2 - 1), \quad (12)$$

is associated with pitchfork bifurcations of elliptic 4-periodic orbits. This is a consequence of the fact that the periodic orbit has a point on the symmetry line $y = x$, see details in the proof of Lemma 1.

- The curve L_4^4 , with equation

$$L_4^4 : 27M_1^2 = 4(M_2 - 2)^3, \quad (13)$$

corresponds to a parabolic bifurcation curve for 4-periodic (non-symmetric) orbits. These orbits are not of Birkhoff type since they are not ordered orbits surrounding the elliptic fixed point $P_{\pi/2}^\pm$.

This curve has a special property. For parameters on L_4^4 with $M_1 > 0$ (resp. $M_1 < 0$) the fixed point $Q_- = (-\sqrt{(M_2 - 2)/3}, -\sqrt{(M_2 - 2)/3})$ (resp. $Q_+ = -Q_-$) of map \mathbf{C}_- is created at a parabolic bifurcation. That is, both parabolic bifurcations, for the 4-periodic orbit and the fixed point, take place simultaneously. See details below. This peculiarity is due to the simple form of the cubic Hénon map and clearly is not a persistent property under arbitrary small perturbations.

- The curves \tilde{L}_4^i , $i = 1, \dots, 4$, are the curves of parabolic 4-periodic orbits with double eigenvalue -1. We have computed these curves numerically. The curves \tilde{L}_4^i , $i = 1, 2, 3$ correspond to period-doubling bifurcations of elliptic 4-periodic orbits.

Remark 1. The curves $L_4^{1,2}$ together with $L_{\pi/2}^-$ reflect a peculiarity of local aspects of the 1:4 resonance in the case of cubic map \mathbf{C}_- . On the other hand, the curves L_4^3 and L_4^4 and the related bifurcations can be considered as peculiarities of the global aspects. Moreover, the curve L_4^4 has no direct relation with the problem of 1:4 resonance since it is a parabolic bifurcation curve for simultaneously two non-symmetric 4-periodic orbits which are symmetric one to other with respect to involution $R : (x, y) \rightarrow (y, x)$.

Let us give further details on how bifurcation curves organize the parameter space. Fix a vertical line $M_1 = C$ with $|C| > 4/3\sqrt{3}$. For parameters on this line, as we change M_2 from bottom to top, one has the following sequence of bifurcations:

- For $C > 4/3\sqrt{3}$ (resp. $C < -4/3\sqrt{3}$) the elliptic 4-periodic orbit created on L_4^1 (resp. L_4^2) becomes hyperbolic when crossing \tilde{L}_4^1 (resp. \tilde{L}_4^2) and, at the crossing of this period-doubling bifurcation curve, an elliptic 8-periodic orbit is born.

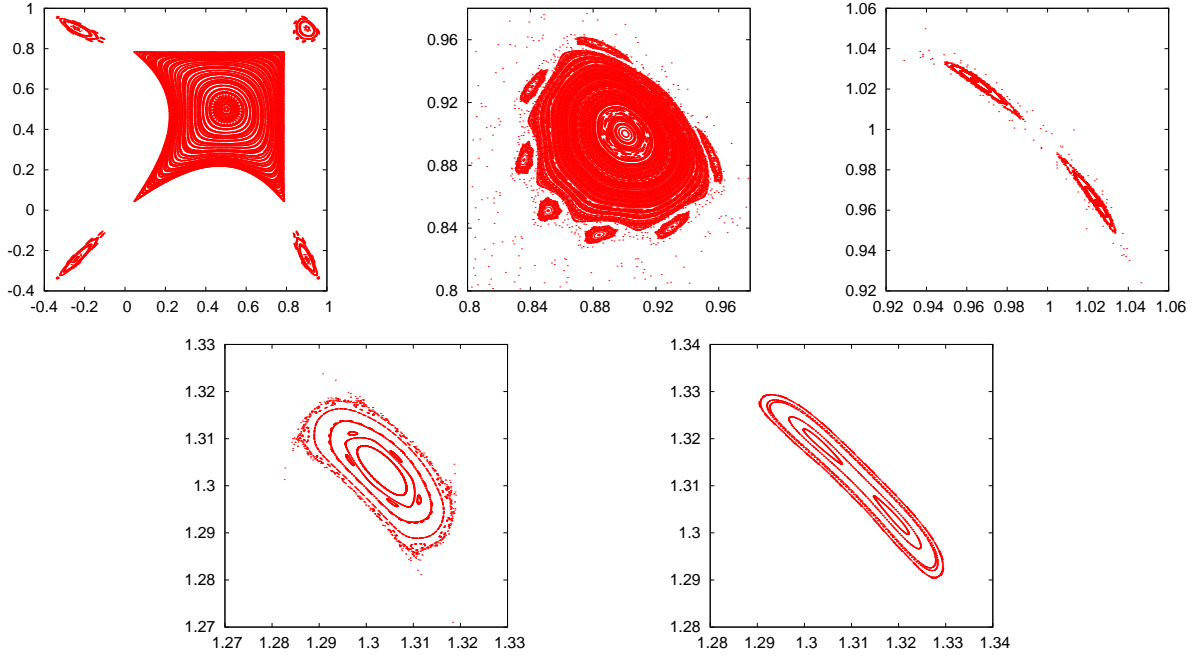


Figure 8: Sequence of bifurcations taking place on the line $M_1 = 0.8$. In the top left plot, for $M_2 = 0.65$, we see the 4-periodic satellite island surrounding the main island around the fixed point. The top center plot is a magnification of the 4-periodic satellite island seen in the top left figure. When increasing M_2 the related elliptic 4-periodic orbit bifurcates. The top right plot is for $M_2 = 0.748$, after the crossing of \tilde{L}_4^1 . The bottom left plot, for $M_2 = 1.36$, and the bottom right, for $M_2 = 1.38$, show the island before and after the pitchfork bifurcation curve L_4^3 .

- For larger M_2 , there appears an elliptic 4-periodic orbit at the inverse period-doubling bifurcation that takes place on \tilde{L}_4^2 (resp. \tilde{L}_4^1).
- This elliptic 4-periodic orbit undergoes a pitchfork bifurcation when crossing L_4^3 and two elliptic 4-periodic orbits persist. The location of the latter elliptic orbits is symmetric with respect to involution $R : (x, y) \rightarrow (y, x)$. See more details in the proof of Lemma 1.
- Those symmetric orbits undergo a period-doubling bifurcation at \tilde{L}_4^3 .

In Fig. 8 we show a sequence of phase space plots where these bifurcations can be observed. The illustrations are for parameters on the vertical line $M_1 = 0.8$. The Fig. 8 top left corresponds to $M_2 = 0.65$, which is located between L_4^1 and \tilde{L}_4^1 . We see the main island around the fixed point and the 4-periodic satellite islands. There are an elliptic 4-periodic orbit and a hyperbolic 4-periodic one (this is located near the peaks of the main stability island, the invariant manifolds of each one of this saddle 4-periodic points surround the corresponding satellite island). In Fig. 8 top center we see a magnification of the 4-periodic satellite island of stability around the elliptic 4-periodic orbit. This elliptic orbit undergoes a period-doubling bifurcation when crossing \tilde{L}_4^1 , the two stability islands can be seen in Fig. 8 top right for $M_2 = 0.748$. Finally the Fig. 8 bottom left and right, for $M_2 = 1.36$ and $M_2 = 1.38$ respectively, illustrate the pitchfork bifurcation taking place when crossing L_4^3 .

Curve L_4^4 is the curve of parabolic 4-periodic orbits with double eigenvalue 1 which is a parabolic bifurcation curve for the 4-periodic orbits. As already said, this curve also coincides with the curve which corresponds to a parabolic bifurcation of the fixed point (or, when $M_1 = 0, M_2 = 2$, to a pitchfork bifurcation of the fixed point). Let us give further details on the sequence of bifurcations when crossing the lines \tilde{L}_4^4 and L_4^4 in Fig. 7 right. To this end consider the vertical line $M_1 = 0.0003$. When moving M_2 from bottom to top in Fig. 7 right one has the following sequence of bifurcations:

- First we have the crossing of \tilde{L}_4^4 . At this crossing two non-symmetric elliptic 4-periodic orbits and two non-symmetric hyperbolic 4-periodic orbits are created as a result of an inverse period-doubling bifurcation. The

position of the two elliptic 4-periodic orbits is shown in Fig. 9 top left. A magnification of one of the satellite islands is shown in Fig. 9 top center.

- When crossing L_4^4 there is a parabolic bifurcation and two new 4-periodic orbits, one elliptic and the other of saddle type, are created. This can be seen in Fig. 9 top right.
- Increasing M_2 , we have two consecutive crossings of \tilde{L}_4^4 . These correspond to period-doubling bifurcations of each of the two elliptic 4-periodic orbits. The two satellite islands after the period-doubling are shown in Fig. 9 bottom left and right, respectively.

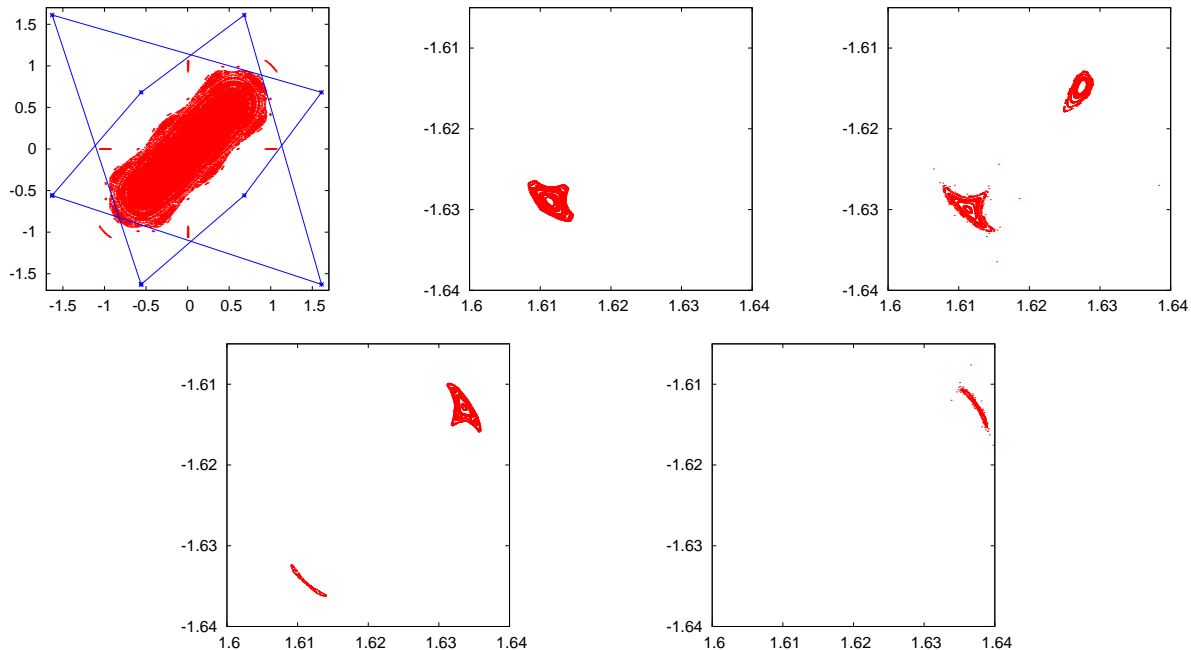


Figure 9: Sequence of bifurcations taking place on the line $M_1 = 0.0003$. Top left: For $M_2 = 2.008$ we see the main island around the fixed point. The lines connect the iterates of the two elliptic 4-periodic orbits. Top center: a magnification of the left plot showing one of the 4-periodic satellite islands. Top right: For $M_2 = 2.0095$ we see the stability islands around one of the iterates of the two elliptic 4-periodic orbits. The new island (at the top right of the plot) is created when crossing the parabolic curve \tilde{L}_4^4 in Fig. 7. Bottom left: For $M_2 = 2.0171$ we see that one of the elliptic 4-periodic orbits undergoes a period-doubling bifurcation. Bottom right: For $M_2 = 2.0232$ the remaining elliptic 4-periodic island undergoes a period-doubling bifurcation.

4 The 1:4 resonance in map C_+ .

Map C_+ has the fixed point $P_{\pi/2}^- = (-\sqrt{-M_2/3}, -\sqrt{-M_2/3})$ (resp. $P_{\pi/2}^+ = -P_{\pi/2}^-$) with eigenvalues $\pm i$ for parameters (M_1, M_2) with $M_1 > 0$ (resp. $M_1 < 0$) on the 1:4 resonance curve

$$L_{\pi/2}^+ : M_1^2 = -\frac{4}{27}M_2(M_2 - 3)^2.$$

The coefficients of normal form (7) around $P_{\pi/2}^\pm$ are $8B_{21}(0) = 3 - 3M_2$, $8B_{03}(0) = 1 + 3M_2$ [Gon05], hence

$$A = \frac{|3 - 3M_2|}{|1 + 3M_2|} = \begin{cases} 1 + \frac{2 - 6M_2}{1 + 3M_2}, & -\frac{1}{3} < M_2 \leq 0, \\ 1 + \frac{4}{|1 + 3M_2|}, & M_2 < -\frac{1}{3}. \end{cases}$$

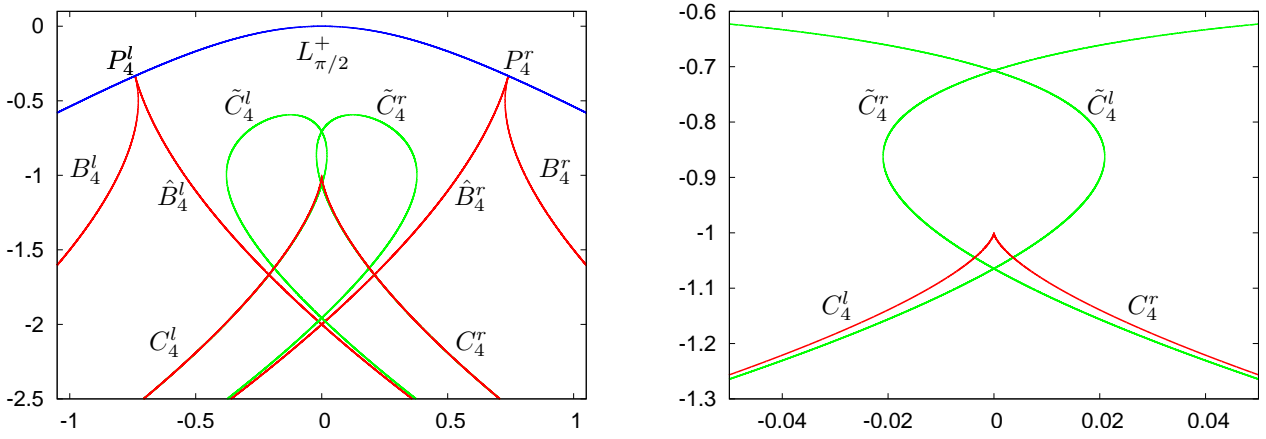


Figure 10: Bifurcation curves in map \mathbf{C}_+ . The right plot is a magnification of the left one near $(0, -1)$.

Since $M_2 \leq 0$ in $L_{\pi/2}^+$, we always have $A > 1$. However, we get degeneracy $B_{03}(0) = 0$ at $M_1 = \pm 20/27$ and $M_2 = -1/3$. These are the points P_4^l and P_4^r in the bifurcation diagram shown in Fig. 10 left where we display in red the bifurcation curves for which there are parabolic 4-periodic orbits with double eigenvalue 1 (either parabolic or pitchfork bifurcations) and in green those curves for which there are 4-periodic orbits with double eigenvalue -1 (hence period-doubling bifurcations).

For parameters (M_1, M_2) above the curve $L_{\pi/2}^+$ the local phase space is topologically equivalent to that of region I in Fig. 5, that is the fixed point $P_{\pi/2}^\pm$ is elliptic and there are no 4-periodic orbits surrounding it.

Crossing the curve $L_{\pi/2}^+$ through $(M_1, M_2) \in L_{\pi/2}^+ \setminus \{P_4^{r,l}\}$ is analogous to cross the line L_2 in Fig. 5 from region I to II. In particular, around $P_{\pi/2}^\pm$ there appear a saddle 4-periodic orbit whose invariant manifolds bound a 4-periodic island of stability with an elliptic 4-periodic orbit inside.

The points $P_4^{l,r}$, corresponding to degeneracy $B_{03} = 0$, are endpoints of the pitchfork bifurcation curves B_4^l, \hat{B}_4^l and B_4^r, \hat{B}_4^r . The explicit equations of such curves are

$$\begin{aligned} B_4^{l,r} : \quad 27M_1^2 &= (3\sqrt{3} - 3\sqrt{-M_2} - 2M_2\sqrt{-M_2})^2, \quad M_2 < -1/3. \\ \hat{B}_4^{l,r} : \quad 27M_1^2 &= 4(2 + M_2)^2(1 - M_2), \quad M_2 < -1/3. \end{aligned} \tag{14}$$

In Fig. 11 we display the sequence of bifurcations taking place when getting inside/outside the region bounded by curves \hat{B}_4^r and B_4^r (by symmetry, bifurcations through B_4^l and \hat{B}_4^l are analogous). For illustrations we choose $M_2 = -0.5$ and change M_1 . For $M_1 = 0.7$ (top left plot in Fig. 11) we see the 4-periodic island having the elliptic point on the symmetry line $y = x$. For parameters on \hat{B}_4^r this point undergoes a pitchfork bifurcation: the elliptic 4-periodic orbit becomes a saddle 4-periodic orbit and a pair of elliptic 4-periodic orbits appear nearby, see Fig. 11 top center. Then the separatrices of the saddle 4-periodic orbits become larger, see Fig. 11 top right, and at some moment between $M_1 = 0.718$ and $M_2 = 0.719$ the separatrices merge⁶ with the exterior separatrices of the other saddle 4-periodic orbits and a sequence of bifurcations related to the reconstruction of homo/heteroclinic connections takes place, see Fig. 11 bottom left. After that, an inverse pitchfork bifurcation occurs, the two elliptic 4-periodic collide into the saddle 4-periodic orbit which becomes elliptic, see Fig. 11 bottom center and right. Note that for $M_1 = 0.73$ the saddle 4-periodic orbit is on the symmetry line $y = x$. This sequence of bifurcations (pitchfork, reconnection of the invariant manifolds and inverse pitchfork) happens generically at the unfolding of the degenerate case $B_{03} = 0$, see details in Appendix B.

⁶Note that for map \mathbf{C}_+ the invariant manifolds are not expected to exactly merge due to the splitting of separatrices.

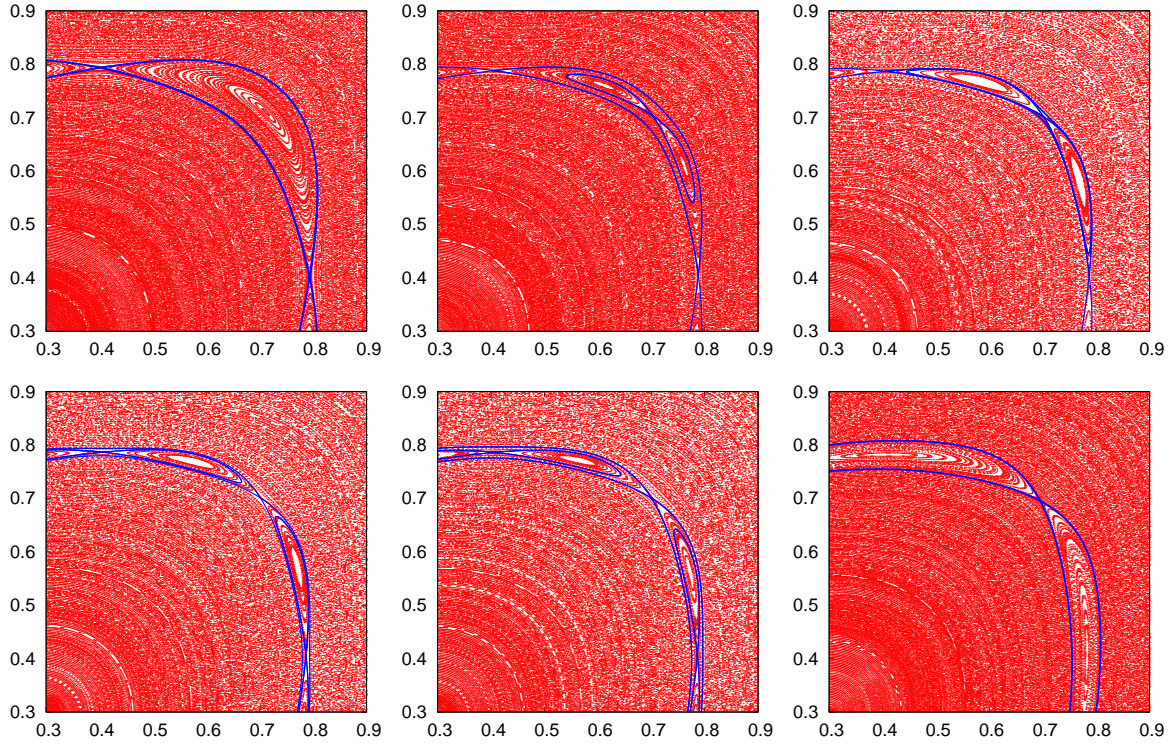


Figure 11: Sequence of bifurcations for fixed $M_2 = -0.5$ in map \mathbf{C}_+ when crossing \hat{B}_4^r and B_4^l . The values of M_1 are: 0.7, 0.715, 0.718 (top), 0.719, 0.72, 0.73 (bottom).

4.1 Other bifurcation curves related to 4-periodic orbits

We have considered some of the local bifurcations of 4-periodic orbits emanating from the 1:4 resonance. The evolution in phase space of the associated 4-periodic orbits leads to other bifurcation curves of other 4-periodic orbits which interact with the obtained ones. In this section we aim to illustrate some aspects of their configuration in parameter space.

Remark 2. The curves $B_4^{l,r}$ and $\hat{B}_4^{l,r}$ are related to the local aspects of the 1:4 resonance. On the other hand, the bifurcations curves considered in this section are not related to the (local) 1:4 resonance problem.

Some of the bifurcation curves to be considered already appear in Fig. 10. The curves $C_4^{r,l}$ correspond to trace= 2 (double eigenvalue 1), given by

$$C_4^{r,l} : 27M_1^2 = -4(1 + M_2)^3, \quad M_2 \leq -1, \quad (15)$$

and the curves $\tilde{C}_4^{r,l}$ to trace= -2 (double eigenvalue -1). To explain the bifurcations that take place let us consider a horizontal line $M_2 = C$, with $C_1 < C < C_2$, where $C_1 \approx -1.6220$ is the M_2 -coordinate of the intersection point between C_4^r and \tilde{C}_4^r (there is only one intersection point, shown in Fig. 10 left) and $C_2 \approx -1.0647$ is the M_2 -coordinate of the bottom intersection point between \tilde{C}_4^r and \tilde{C}_4^l shown in the Fig. 10 right. When varying M_1 from right to left in Fig. 10 one has the following bifurcation sequence:

- For M_1 in the right hand side of \hat{B}_4^r there are saddle 4-periodic orbits along with a pair of elliptic 4-periodic orbits. Recall that curve \hat{B}_4^r corresponds to a pitchfork bifurcation, hence to the left of this curve we get a 4-periodic island of stability creating a garland containing saddle and elliptic 4-periodic orbits.
- When decreasing M_1 , an inverse period-doubling bifurcation occurs at the first crossing with curve \tilde{C}_4^r in Fig. 10 left. The bifurcation is as follows: for parameters to the right of \tilde{C}_4^r , in a neighborhood of the elliptic 4-periodic orbit, there appears a saddle 8-periodic orbit. This 8-periodic orbit bifurcates from the saddle 4-periodic orbit that remains to the left of \tilde{C}_4^r .

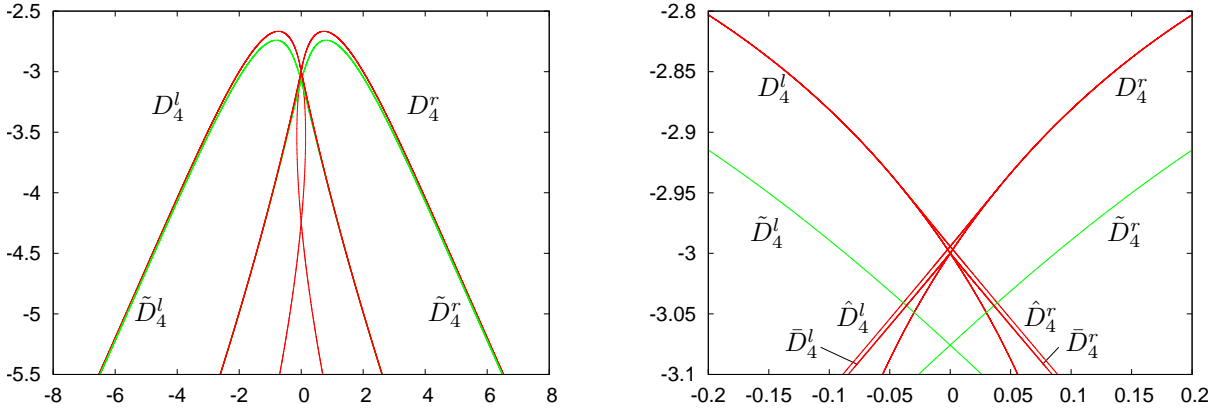


Figure 12: Other bifurcation curves of 4-periodic orbits in map \mathbf{C}_+ . In the left plot we see the two (green) curves $\tilde{D}_4^{l,r}$ that correspond to parabolic 4-periodic orbits with double eigenvalue -1 . The curves $D_4^{l,r}$ correspond to period-doubling of 2-periodic orbits. The other curves are better seen in the right plot, which is a magnification of the left one. In the right plot we see that curves $\hat{D}_4^{l,r}$, corresponding to parabolic 4-periodic with double eigenvalue 1 respectively, become tangent to $D_4^{l,r}$. Finally, curves $\bar{D}_4^{l,r}$, which correspond to a pitchfork bifurcation of 4-periodic orbits, end up at $(M_1, M_2) = (0, -3)$.

- For parameters on the curve C_4^r , a parabolic bifurcation for a 4-periodic orbit takes place. At this bifurcation a saddle and an elliptic 4-periodic orbits are created. One of the pairs of the elliptic and hyperbolic 4-periodic orbits that bifurcate lie on the symmetry line $y = x$. The elliptic orbit undergoes a period-doubling bifurcation when crossing the curve \tilde{C}_4^r . See Fig. 10 right.

We have found other bifurcation curves related to 4-periodic orbits. We note that the corresponding 4-periodic orbits do not lie on the symmetry line $y = x$ of map \mathbf{C}_+ . The bifurcation curves are shown in Fig. 12 left. Note that, in the left plot, curves $D_4^{l,r}$, which wrap the full structure of bifurcation curves shown, are confined in the region below the curve $L_{\pi/2}^+$ partially shown in Fig. 10. Let us give some details on the bifurcation curves obtained.

- The curves $D_4^{l,r}$ are given by

$$D_4^{l,r} : \pm M_1 = \sqrt{\frac{-M_2}{3}} \left(\frac{2}{3} M_2 + 1 \right) \pm \sqrt{-3M_2 - 8},$$

and they correspond to period-doubling bifurcation curves of 2-periodic orbits. The bifurcation curves related to 2-periodic orbits were studied in [GGO17], in particular, curves $D_4^{l,r}$ were obtained there (they correspond to the ones denoted by L_2^{-1} and L_2^{-2} in [GGO17]).

- The bifurcation curves $\hat{D}_4^{l,r}$ correspond to a parabolic bifurcation of 4-periodic orbits. The curve \hat{D}_4^l ends up in a point $(M_1, M_2) = (M_1^*, M_2^*) \approx (0.041064, -2.944529)$ where it becomes tangent to the curve D_4^l . See details in Fig. 12 right. When $(M_1, M_2) \in \hat{D}_4^l$ tends to (M_1^*, M_2^*) the 4-periodic orbit approaches the 2-periodic orbit that undergoes the period-doubling bifurcation in D_4^l .
- The bifurcation curves $\bar{D}_4^{l,r}$, whose equations are

$$\bar{D}_4^{l,r} : 27M_1^2 = \left(3\sqrt{3} + 3\sqrt{-M_2} + 2M_2\sqrt{-M_2} \right)^2, \quad M_2 \leq -3, \quad (16)$$

correspond to a pitchfork bifurcation of 4-periodic orbits. The curve \bar{D}_4^l ends up at the point $(M_1, M_2) = (0, -3)$ where curves D_4^l and D_4^r intersect.

- Finally, the bifurcation curves $\tilde{D}_4^{l,r}$ correspond to 4-periodic orbits with double eigenvalue -1 , hence they are period-doubling bifurcation curves of 4-periodic orbits.

To provide further details of the sequence of bifurcations that take place we consider the horizontal line $M_2 = -3.1$ and, on this line, different values of $M_1 < 0$. We refer to Fig. 12 right to see the location of the different bifurcation

curves. To start with we consider $M_1 = -0.047$, which is between the curves D_4^r and \tilde{D}_4^r . For parameter values $(M_1, M_2) = (-0.047, -3.1)$ the phase space shows up a 2-periodic island and a 4-periodic island (which is a 2-periodic satellite of the 2-periodic island). Denote by e_2 (resp. by e_4) the elliptic points around which the 2-periodic (resp. the 4-periodic) islands of stability are organized. The 2-periodic elliptic island, for $M_2 = -3.1$, persists⁷ for $-0.047 < M_1 \leq 0$. When changing M_1 on the line $M_2 = -3.1$, the following bifurcations are observed:

- At the crossing of \tilde{D}_4^r from left to right, the point e_4 undergoes a period-doubling bifurcation, and an 8-periodic elliptic point is created.
- When crossing D_4^r from right to left, the point e_2 undergoes a period-doubling. Consequently, a 4-periodic elliptic orbit is born, denote it by \tilde{e}_4 .
- At the crossing of \bar{D}_4^l from right to left, there is an inverse pitchfork bifurcation at which the two 4-periodic elliptic points e_4 and \tilde{e}_4 collide and give rise to a 4-periodic elliptic orbit. This 4-periodic elliptic orbit persists until the crossing of \hat{D}_4^l where disappears at a parabolic bifurcation.

Other sequences of bifurcations can be observed for other lines $M_2 = C$ (specially when considering M_2 in the range shown in Fig. 12 right). For example, for $M_2 = -2.9$ and moving M_1 from right to left starting from $M_1 = 0$, one has that the 2-periodic elliptic orbit undergoes a period-doubling bifurcation at D_4^l (roughly for $M_1 \approx -0.1$). The 4-periodic elliptic orbit that bifurcates from the previous bifurcation undergoes a period-doubling at \tilde{D}_4^l (which happens for $M_1 < -0.2$).

As a final comment, we note that the bifurcation curves considered before allow us to explain the sequences of bifurcations of 4-periodic orbits that we have observed when plotting the islands of stability for different values of (M_1, M_2) . Hence, we believe that the bifurcation diagram for the 4-periodic orbits in the (M_1, M_2) regions shown is complete (although we have no proof of this fact).

5 Conclusions and related topics

We have obtained a detailed picture of the bifurcation diagrams near the 1:4 resonance of maps \mathbf{C}_\pm in (1)-(2). A description of the bifurcations taking place when crossing the main bifurcation curves derived (either analytically or numerically) has been provided. Special emphasis has been put to the clarification of the scenarios related to the degeneracies of the 1:4 normal form. We have shown that degeneracy $A = 1$ happens for \mathbf{C}_- while degeneracy $B_{03} = 0$ happens for \mathbf{C}_+ , and we have analysed the dynamical consequences of these degeneracies in these concrete cases.

We believe that the results presented in this work are relevant for related studies. Namely, we want to emphasize that the study of the cubic Hénon maps (1) and (2) (and naturally the quadratic one (3)) is important because

- these maps are the simplest nonlinear symplectic maps of the plane, and therefore the understanding of the basic properties of the dynamics and the bifurcations in such maps will be very useful in more general contexts.
- as pointed out in the introduction, these maps are, in fact, normal forms of the first return maps near the quadratic (map (3)) and cubic (maps (1) and (2)) homoclinic tangencies: it is easy to relate the structure of the bifurcations of these maps with the global bifurcations happening at the homoclinic tangency.

However, there is another important reason why the 1:4 resonance in the cubic Hénon maps is of interest. It is connected with mixed dynamics – a new third type of dynamical chaos characterized by the principal inseparability of attractors from repellers⁸ and from the conservative elements of dynamics (for example, periodic sinks, sources and elliptic points), see e.g. [GST97, LS04, DGGLS13, Gon16, GT17]. It is worth noting that the mixed dynamics can be an open property of reversible non-conservative chaotic systems in which self-symmetric orbits are conservative (e.g., symmetric elliptic trajectories), while asymmetric ones appear in pairs and have the opposite type of stability (e.g., “sink-source” pairs). Such symmetric/asymmetric orbits emerge usually as a result of various homoclinic bifurcations, see more details in [DGGLS13], including local symmetry breaking bifurcations like reversible pitchfork ones [LT12].

⁷If one considers $M_2 < 4$, the 2-periodic elliptic point persists when moving M_1 from right to left until crossing a parabolic bifurcation curve of 2-periodic orbits. This curve was obtained in [GG017] and was denoted there by L_2^+ .

⁸Here attractor and repeller are considered in the Conley-Ruelle sense [Con78, Rue81], see also [GT17].

However, the structure of such bifurcations in many cases is not known, as happens for example in the case of symmetric cubic homoclinic tangencies. It can be deduced from [GGO17] that the first return map near a symmetric cubic homoclinic tangency must coincide in the main order with the cubic Hénon map either of form (1) or (2) which are reversible maps. When studying the problem of 1:4 resonance in these maps, we have shown that pitchfork bifurcations appear accompanying the resonance local bifurcation. These bifurcations should lead to the birth of a “sink-source” pair of periodic orbits in general reversible contexts.

We believe that these topics certainly deserve future devoted studies and we hope that the results presented here will contribute to facilitate them.

Acknowledgments

The paper is carried at the financial support of the RSF grant 14-41-00044. AV and MG has been supported by the Spanish grant MTM2016-80117-P (MINECO/FEDER, UE). AV also thanks the Catalan grant 2014-SGR-1145. MG also thanks the Juan de la Cierva-Formación Fellowship FJCI-2014-21229 and the MICIIN/FEDER grant MTM2015-65715-P. SG thanks the Russian Foundation for Basic Research, grant 16-01-00364, and the Russian Ministry of Science and Education, project 1.3287.2017 – target part, for supporting the scientific research. IO points out that this paper is a contribution to the project M2 (Systematic multiscale modelling and analysis for geophysical flow) of the Collaborative Research Centre TRR 181 “Energy Transfer in Atmosphere and Ocean” funded by the German Research Foundation.

A Bifurcation curves associated with parabolic 4-periodic orbits in \mathbf{C}_\pm

In this section we derive some of the equations of the bifurcation curves displayed in Fig. 7, 10 and 12. These curves correspond to the appearance of parabolic 4-periodic orbits in maps (1) and (2).

The curves corresponding to trace= 2 are given by the following lemma.

Lemma 1. *The following bifurcation curves corresponding to parabolic 4-periodic orbits with double eigenvalue 1 exist:*

1. For map \mathbf{C}_- (1), curves L_4^i , $i = 1, 2, 3, 4$, displayed in Fig. 7, are given by the equations (11), (12) and (13).
2. For map \mathbf{C}_+ (2), curves $B_4^{l,r}$, $\hat{B}_4^{l,r}$ and $C_4^{l,r}$, displayed in Fig. 10. They are given by (14) and (15). Moreover, the curves $\bar{D}_4^{l,r}$, displayed in Fig. 12, are given by (16). Also, curves $\hat{D}_4^{l,r}$, displayed in Fig. 12, satisfy the relations (27).

Proof. We rewrite maps (1) and (2) in the form

$$\begin{pmatrix} \bar{x} \\ \bar{y} \end{pmatrix} = \mathbf{C}_\pm \begin{pmatrix} x \\ y \end{pmatrix} = \begin{pmatrix} y \\ -x + P(y) \end{pmatrix}.$$

where $P(y) = M_1 + M_2y - \delta y^3$, being $\delta = 1$ in case of map (1) and $\delta = -1$ in case of map (2). The point Q is a parabolic 4-periodic orbit with trace 2 for \mathbf{C}_\pm if the following conditions are satisfied:

$$(a) \mathbf{C}_\pm^4(Q) = Q \text{ and } (b) \text{tr } D(\mathbf{C}_\pm^4(Q)) = 2, \quad (17)$$

where D stands for the Jacobi matrix.

Condition (a) is obviously equivalent to $\mathbf{C}_\pm^{-2}(Q) = \mathbf{C}_\pm^2(Q)$, which yields

$$(y^2 - yP(x) + P^2(x) - \delta M_2)(-2y + P(x)) = 0, \quad (x^2 - xP(y) + P^2(y) - \delta M_2)(-2x + P(y)) = 0, \quad (18)$$

where (x, y) are the coordinates of the point Q . It is easy to check that if $(-2y + P(x)) = 0$ and $(-2x + P(y)) = 0$ simultaneously, Q is actually either a 2-periodic orbit or a fixed point. For this reason, for 4-periodic orbits, we assume that at least one of these expressions is non-zero. Then, we get two different cases, which we consider separately:

Case 1. $(-2y + P(x)) \neq 0$ and $(-2x + P(y)) \neq 0$;

Case 2. $(-2y + P(x)) = 0$, $(-2x + P(y)) \neq 0$ (the case when $(-2x + P(y)) = 0$, $(-2y + P(x)) \neq 0$ is considered analogously).

In Case 1, equations (18) are rewritten as follows

$$y^2 - yP(x) + P^2(x) = \delta M_2, \quad x^2 - xP(y) + P^2(y) = \delta M_2. \quad (19)$$

The last equations show that pairs $(y, P(x))$ and $(x, P(y))$ are the coordinates of points on the ellipse given by equation $X^2 - XY + Y^2 = \delta M_2$, and that (19) has solutions for $M_2 \geq 0$ in case of \mathbf{C}_- and for $M_2 \leq 0$ in case of \mathbf{C}_+ . Thus, we introduce the parametrization with parameters t_1 and t_2 along this ellipse in such a way that for some $-\pi \leq t_1, t_2 \leq \pi$ we have:

$$\begin{aligned} y &= \sqrt{\delta \frac{M_2}{3}} \cos t_1 - \sqrt{\delta M_2} \sin t_1, & x &= \sqrt{\delta \frac{M_2}{3}} \cos t_2 - \sqrt{\delta M_2} \sin t_2, \\ P(x) &= 2\sqrt{\delta \frac{M_2}{3}} \cos t_1, & P(y) &= 2\sqrt{\delta \frac{M_2}{3}} \cos t_2. \end{aligned} \quad (20)$$

The values of $x, y, P(x), P(y)$ given by the parametrization (20) satisfy

$$\begin{aligned} 2\sqrt{\delta \frac{M_2}{3}} \cos t_1 = P(x) &= P\left(\sqrt{\delta \frac{M_2}{3}} \cos t_2 - \sqrt{\delta M_2} \sin t_2\right) = M_1 + \frac{2}{3\sqrt{3}} M_2 \sqrt{\delta M_2} \cos 3t_2, \\ 2\sqrt{\delta \frac{M_2}{3}} \cos t_2 = P(y) &= P\left(\sqrt{\delta \frac{M_2}{3}} \cos t_1 - \sqrt{\delta M_2} \sin t_1\right) = M_1 + \frac{2}{3\sqrt{3}} M_2 \sqrt{\delta M_2} \cos 3t_1. \end{aligned} \quad (21)$$

Condition (b) in (17) gives us the equation

$$[P'(y) + P'(-y + P(x))][P'(x) + P'(-x + P(y))] = P'(y)P'(-y + P(x))P'(x)P'(-x + P(y)), \quad (22)$$

which, using the parametrization (20), is rewritten as

$$16M_2^2 \sin^2 t_1 \sin^2 t_2 [1 - M_2^2(1 + 2 \cos 2t_1)(1 + 2 \cos 2t_2)] = 0, \quad (23)$$

therefore either $|\cos t_{1,2}| > 1/2$ or $|\cos t_{1,2}| < 1/2$.

Thus, we get 3 equations, (21) and (23), for variables t_1, t_2, M_1, M_2 and, in order to obtain the desired bifurcation curves, we just need to exclude t_1 and t_2 .

Consider first Case 1.1 when $\cos t_1 = \cos t_2$. With this, equations (21) completely coincide and the parametric equation of the bifurcation curve is the following

$$M_1 = \frac{2}{3\sqrt{3}} \sqrt{\delta M_2} (3 \cos t_1 - M_2 \cos 3t_1), \quad M_2 = \frac{\delta}{|1 + 2 \cos 2t_1|}, \quad 0 < t_1 < \pi.$$

Excluding $\cos t_1$, we obtain the explicit formulas of the curves, namely: in the case \mathbf{C}_- , we get L_4^1 for $0 < t_1 < \pi/3$, L_4^3 for $\pi/3 < t_1 < 2\pi/3$ and L_4^2 for $2\pi/3 < t_1 < \pi$, while in the case \mathbf{C}_+ , we get \hat{B}_4^r for $0 < t_1 < \pi/3$, $C_4^{r,l}$ for $\pi/3 < t_1 < 2\pi/3$ and \hat{B}_4^l for $2\pi/3 < t_1 < \pi$.

Consider next Case 1.2 when $\cos t_1 \neq \cos t_2$, then equations (21) can be solved with respect to M_1 and M_2 :

$$M_1 = \frac{2}{3\sqrt{3}} \sqrt{\delta M_2} (3 \cos t_2 - M_2 \cos 3t_1), \quad M_2 = \frac{3(\cos t_1 - \cos t_2)}{\cos 3t_2 - \cos 3t_1}. \quad (24)$$

Plugging M_2 into equation (23) we obtain the following relation between t_1 and t_2

$$4 \cos^2 t_1 + 16 \cos t_1 \cos t_2 + 4 \cos^2 t_2 + 3 = 0,$$

where one can see that variables $\cos t_1$ and $\cos t_2$ satisfy the equation of a hyperbola $4X^2 + 16XY + 4Y^2 + 3 = 0$. Thus, they can be parametrized in the following way:

$$\cos t_1 = \frac{\sqrt{2}}{8}(1 - \sqrt{3})t - \frac{\sqrt{2}}{8}(1 + \sqrt{3})\frac{1}{t}, \quad \cos t_2 = \frac{\sqrt{2}}{8}(1 + \sqrt{3})t - \frac{\sqrt{2}}{8}(1 - \sqrt{3})\frac{1}{t}.$$

The natural conditions $|\cos t_{1,2}| \leq 1$ are fulfilled only for $t_- \leq |t| \leq t_+$, where $t_{\pm} = \frac{\sqrt{3} \pm 1}{\sqrt{2}}$. Substituting this parametrization into (24) and excluding t gives the curve L_4^4 in the case \mathbf{C}_- . Note that for this parametrization, we have $M_2 = -\frac{4t^2}{t^4 - 4t^2 + 1}$ which takes only positive values for $t_- \leq |t| \leq t_+$, and this case does not provide any bifurcation curve for \mathbf{C}_+ .

In Case 2 we get the equations $2y = P(x)$, $x^2 - xP(y) + P^2(y) = \delta M_2$ and the equation (22). The second one admits the parametrization as before (note that $t \neq n\pi$, otherwise we have $2x = P(y)$, i.e. a 2-periodic orbit or a fixed point):

$$x = \sqrt{\delta \frac{M_2}{3}} \cos t - \sqrt{\delta M_2} \sin t, \quad P(y) = 2\sqrt{\delta \frac{M_2}{3}} \cos t,$$

and equation (22) is written as

$$2(M_2 - 3\delta y^2)(-4M_2 \sin^2 t) = (M_2 - 3\delta y^2)^2(-4M_2^2 \sin^2 t)(1 + 2 \cos 2t). \quad (25)$$

Let us consider Case 2.1, when $M_2 - 3\delta y^2 = 0$ in (25), i.e. $y = \pm \sqrt{\delta \frac{M_2}{3}}$. Then we have

$$\begin{aligned} 2\sqrt{\delta \frac{M_2}{3}} \cos t = P(y) &= M_1 \pm \frac{2}{3\sqrt{3}} M_2 \sqrt{\delta M_2}, \\ \pm 2\sqrt{\delta \frac{M_2}{3}} = P(x) &= M_1 + \frac{2}{3\sqrt{3}} M_2 \sqrt{\delta M_2} \cos 3t. \end{aligned}$$

The possible bifurcation curves are given parametrically in the following form

$$M_2 = -\frac{3}{(2 \cos t \pm 1)^2}, \quad M_1 = 2\sqrt{\delta \frac{M_2}{3}} \cos t \mp \frac{2}{3\sqrt{3}} M_2 \sqrt{\delta M_2}. \quad (26)$$

Since $M_2 < 0$, the equations (26) do not give any curve for the map \mathbf{C}_- . In the case of \mathbf{C}_+ we obtain the equations for curves $B_4^{l,r}$ (which corresponds to the branch that is obtained for $t \in [0, 2\pi/3)$) and the equations for the curves $\bar{D}_4^{l,r}$ (for $t \in (2\pi/3, \pi]$).

For the Case 2.2, when $M_2 - 3\delta y^2 \neq 0$ in (25), we have the equations

$$\begin{aligned} 2 &= (M_2 - 3\delta y^2)M_2(1 + 2 \cos 2t), \\ 2\sqrt{\delta \frac{M_2}{3}} \cos t = P(y) &= M_1 + M_2 y - \delta y^3, \\ M_1 + \frac{2}{3\sqrt{3}} M_2 \sqrt{\delta M_2} \cos 3t = P(x) &= 2y. \end{aligned} \quad (27)$$

We have numerically checked that $\hat{D}_4^{l,r}$ fulfill these implicit equations. □

Concerning parabolic 4-periodic orbits with double eigenvalue -1 (trace = -2), an analogous proof to the previous Lemma can be done. The only difference that condition (b) in (17) now is $\text{tr } D(\mathbf{C}_{\pm}^4(Q)) = -2$ which gives instead of (22) and (23) the third equation

$$[P'(y) + P'(-y + P(x))][P'(x) + P'(-x + P(y))] = P'(y)P'(-y + P(x))P'(x)P'(-x + P(y)) + 4, \quad (28)$$

that, using the parametrization (20) in Case 1, is rewritten as

$$16M_2^2 \sin^2 t_1 \sin^2 t_2 [1 - M_2^2(1 + 2 \cos 2t_1)(1 + 2 \cos 2t_2)] = 4. \quad (29)$$

Thus, the bifurcation curves \tilde{L}_4^i , $i = 1, 2, 3, 4$, $\tilde{C}_4^{l,r}$ and $\tilde{D}_4^{l,r}$, displayed in Figs. 7, 10 and 12, respectively, should satisfy the equations (21) and (28). For example, in the simplest case $\cos t_1 = \cos t_2$, which is analogous to Case 1.1 in the proof of Lemma 1, the equation (29) becomes

$$4M_2^2 \sin^4 t_1 [1 - M_2^2(1 + 2 \cos 2t_1)^2] = 1,$$

which makes sense for M_2 to exist for $|\cos t_1| \leq \sqrt{2/5}$. Using the last equation as well as (21), we get the parametric expression

$$M_1 = \frac{2}{3\sqrt{3}} \sqrt{\delta M_2} (3 \cos t_1 - M_2 \cos 3t_1), \quad M_2 = \delta \frac{\sqrt{\sin^2 t_1 \pm \sqrt{\sin^4 t_1 - (1 + 2 \cos(2t_1))^2}}}{2|1 + 2 \cos 2t_1| |\sin t_1|},$$

where $\arccos \sqrt{2/5} \leq t_1 \leq \arccos(-\sqrt{2/5})$. The parametric expression gives the curves $\tilde{L}_4^{1,2}$ (note that for $t_1 = \pi/2$ the curves have the intersection point $M_1 = 0, M_2 = 1/\sqrt{2}$), in the case of map \mathbf{C}_- , and the curves $\tilde{C}_4^{l,r}$ (as well for $t_1 = \pi/2$ the curves intersect at $M_1 = 0, M_2 = -1/\sqrt{2}$), in the case of map \mathbf{C}_+ .

The other cases (analogous to Cases 1.2, 2.1 and 2.2 in the proof of Lemma 1) lead to cumbersome equations that we omit.

B Local analysis of the 1:4 resonance with degeneracy $B_{03} = 0$

Consider a one-parameter family $F_\delta : \mathbb{R}^2 \rightarrow \mathbb{R}^2$ of area-preserving maps which admit the reversibility $(x, y) \rightarrow (y, x)$. Let us consider $\delta \in \mathbb{R}$, small enough, being a parameter that unfolds a 1:4 resonant fixed point. Without loss of generality, we assume $F_\delta(0) = 0$ and $\text{Spec} DF_0(0) = \pm i$. There exists a (formal) change of coordinates such that it reduces F_δ to its Takens normal form N_δ (see [Tak74, Bro90]) which commutes with the linearized map Λ_0 of F_0 at 0, that is,

$$N_\delta \circ \Lambda_0 = \Lambda_0 \circ N_\delta$$

The normal form is easily expressed in terms of complex conjugated variables $z = x + iy$, $z^* = x - iy$. The map $\Lambda_0^{-1} N_\delta$ is near-the-identity and can be (formally) interpolated by a Hamiltonian flow, that is,

$$\Lambda_0^{-1} N_\delta = \phi_{H_\delta}^{t=1},$$

where the Hamiltonian function H_δ is Λ_0 -invariant and is the sum of resonant terms

$$H_\delta(z, z^*) = \sum_{j-k \in \Gamma} h_{j,k} z^j (z^*)^k,$$

being

$$\Gamma = \{s \in \mathbb{Z}, s \equiv 0 \pmod{4}\}$$

the set of resonant monomials.

The area-preserving condition implies that coefficients $h_{i,i}$ are real. Moreover, the reversibility $(x, y) \rightarrow (y, x)$ imply that $h_{ij} = h_{ij}^*$. Then, by introducing Poincaré polar (symplectic) coordinates

$$I = \frac{|z|^2}{2}, \quad \varphi = \arg(z),$$

the interpolating Hamiltonian is reduced to

$$H(I, \varphi) = b_1 I + b_2 I^2 + b_3 I^3 + \mu I^2 \cos(4\varphi) + B I^3 \cos(4\varphi + \varphi_1) + \mathcal{O}(I^4),$$

where all the coefficients are real and depend on δ , and φ_1 is an initial phase.

We are interested in the analysis of the unfolding of the degenerate case (i.e. the situation with $B_{03} = 0$). This means that $b_1 = \mu = 0$ at the exact resonance (when $\delta = 0$). Note that it is natural to adjust the angle variable so that $\varphi_1 = 0$. Taking into account that $b_1 = \delta$ one has

$$H(I, \varphi) = \delta I + b_2 I^2 + b_3 I^3 + \mu I^2 \cos(4\varphi) + B I^3 \cos(4\varphi) + \mathcal{O}(I^4).$$

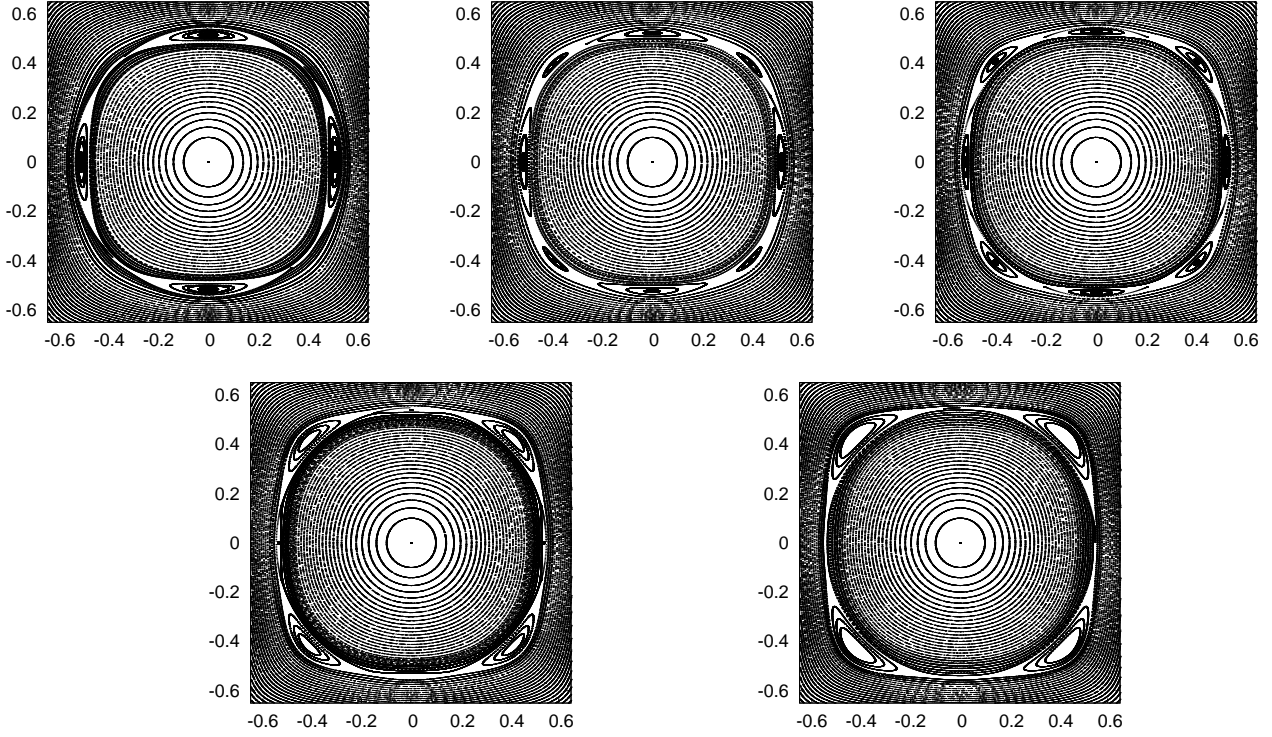


Figure 13: We show the phase space for $\delta = -0.28, -0.29, -0.3$ (first row) and $\delta = -0.31, -0.32$ (second row) for the selected values of the parameters, see text for details.

Our goal is to describe the bifurcations when $\delta, \mu \neq 0$ but small. Note that this degenerate 1:4 resonance case leads to a codimension two bifurcation problem.

Ignoring higher order terms in I , the equations are

$$\dot{I} = -\frac{\partial H}{\partial \varphi} = 4\mu I^2 \sin(4\varphi) + 4BI^3 \sin(4\varphi) + \mathcal{O}(I^4), \quad (30)$$

$$\dot{\varphi} = \frac{\partial H}{\partial I} = \delta + 2b_2 I + 3b_3 I^2 + 2\mu I \cos(4\varphi) + 3BI^2 \cos(4\varphi) + \mathcal{O}(I^3). \quad (31)$$

We look for fixed points (I_*, φ_*) with $I_* > 0$. Requiring $\dot{I} = 0$ one obtains

$$I_* = -\frac{\mu}{B} + \mathcal{O}(\mu^2),$$

and substituting it into the equation $\dot{\varphi} = 0$ gives

$$(2\mu I_* + 3BI_*^2) \cos(4\varphi) = -(\delta + 2b_2 I_*) + \mathcal{O}(\mu^2),$$

which, fixed a small value of μ , determines a small range of values of δ (close to $-2b_2 I_*$) for which there are fixed points. These are non-symmetric points which are created and disappear in pitchfork bifurcations. See [GLRT14] for related comments. One has

$$I_* = -\frac{\mu}{B}, \quad \cos(4\varphi_*) = -\frac{B}{\mu^2} \left(b_1 - 2b_2 \frac{\mu}{B} \right).$$

For illustrations, we consider $b_2 = 1, b_3 = 0, B = 1, \mu = -0.15$. The phase spaces for $\delta = -0.28, -0.29, -0.3, -0.31$ and -0.32 are shown in Fig. 13.

References

[Arn88] V.I. Arnold. Geometrical Methods in the Theory of Ordinary Differential Equations. *Springer*; 2nd edition, 1988.

- [AAIS86] Arnold V., Afraimovich V., Ilyashenko Yu., Shilnikov L., Bifurcation theory, *Dynamical Systems* v.5, Moscow, 1986.
- [Bir87] V. S. Biragov. Bifurcations in a two-parameter family of conservative mappings that are close to the Hénon mapping. (Russian) [Translated in *Selecta Math. Soviet.* 9(3):273–282, 1990.] *Methods of the qualitative theory of differential equations*, 10–24, 1987.
- [Bro90] H. Broer. Notes on perturbation theory. *Series of Scientific Monographies “Mathematics and fundamental applications”*, 1990.
- [BS89] V.S. Biragov, L.P. Shilnikov. On the bifurcation of a saddle-focus separatrix loop in a three-dimensional conservative dynamical system. (Russian) [Translated in *Selecta Math. Soviet.* 11(4):333–340, 1992.] *Methods in qualitative theory and bifurcation theory*, 2534, 1989.
- [Con78] C. Conley. Isolated Invariant Sets and the Morse Index. CBMS Reg. Conf. Ser. Math., 38. *Amer. Math. Soc., Providence, RI*, 1978.
- [DGG15] A. Delshams, M. Gonchenko, S. Gonchenko. On dynamics and bifurcations of area-preserving maps with homoclinic tangencies. *Nonlinearity*, 28(9):3027–3071, 2015.
- [DGGLS13] A. Delshams, S.V. Gonchenko, V.S. Gonchenko, J.T. Lázaro, O.V. Sten’kin. Abundance of attracting, repelling and elliptic orbits in two-dimensional reversible maps. *Nonlinearity*, 26(1):1-33, 2013.
- [DM00] H.R. Dullin, J.D. Meiss. Generalized Hénon maps: the cubic diffeomorphisms of the plane. *Phys. D*, 143:262-289, 2000.
- [GG09] M. Gonchenko, S. Gonchenko. On cascades of elliptic periodic orbits for area-preserving maps close to a map with a homoclinic tangency, *Regul. Chaotic Dyn.*, 14(1):116-136, 2009.
- [GG14] V. Gelfreich, N. Gelfreich. Unique normal forms near a degenerate elliptic point in two-parametric families of area-preserving maps. *Nonlinearity*, 27(7):1191-1245, 2014.
- [GGO17] M, Gonchenko, S. Gonchenko, I. Ovsyannikov. Bifurcations of cubic homoclinic tangencies in two-dimensional symplectic maps. *Math. Model. Nat. Pheno.*, 12(1):41-61, 2017.
- [GK88] S.V. Gonchenko, Yu.A. Komlev. Bifurcations and chaos in cubic maps of the plane. (Russian) *Methods of the Qualitative Theory of Differential Equations*, pp 33-40, 1988.
- [GLRT14] S.V. Gonchenko, J.S.W. Lamb, I. Rios, D. Turaev. Attractors and repellers near generic elliptic points of reversible maps. *Dokl. Math.*, 89(1):65-67, 2014.
- [Gon85] S.V. Gonchenko. On a two parameter family of systems close to a system with a nontransversal Poincaré homoclinic curve. I. (Russian) [Translated in *Selecta Math. Soviet.*, 10(1):69-80, 1991] *Methods of Qualitative Theory of Differential Equations*, 55-72, 1985.
- [Gon05] M.S. Gonchenko. On the structure of 1:4 resonances in Hénon maps, *Internat. J. Bifur. Chaos Appl. Sci. Engrg.*, 15(11):3653-3660, 2005.
- [Gon16] S. Gonchenko. Reversible Mixed Dynamics: A Concept and Examples. *Discontinuity, Nonlinearity, and Complexity*, 5(4):365-374, 2016.
- [GST96] S. V. Gonchenko, L. P. Shilnikov, D. V. Turaev. Dynamical phenomena in systems with structurally unstable Poincaré homoclinic orbits, *Chaos*, 6(1):15-31, 1996.
- [GST97] S.V. Gonchenko, L.P. Shilnikov, D.V. Turaev. On Newhouse regions of two-dimensional diffeomorphisms close to a diffeomorphism with a nontransversal heteroclinic cycle, *Proc. Steklov Inst. Math.*, 216:7-118, 1997.
- [GSV13] S.V. Gonchenko, C. Simó, A. Vieiro. Richness of dynamics and global bifurcations in systems with a homoclinic figure-eight. *Nonlinearity*, 26(3):621–678, 2013.
- [GT17] S.V. Gonchenko, D.V. Turaev. On three types of dynamics and the notion of attractor. (Russian) [Translated in *Proc. Steklov Inst. Math.*, 297:116137, 2017] *Tr. Mat. Inst. Steklova, Poryadok i Khaos v Dinamicheskikh Sistemakh*, 297:133157, 2017.

- [Kra94] B. Krauskopf. The bifurcation set for the 1:4 resonance problem. *Experiment. Math.*, 3(2):107-128, 1994.
- [Kuz95] Yu. Kuznetsov. Elements of applied bifurcation theory. Applied Mathematical Sciences, 112. *Springer-Verlag, New York*, 1995.
- [LS04] J.S.W. Lamb, O.V. Stenkin. Newhouse regions for reversible systems with infinitely many stable, unstable and elliptic periodic orbits, *Nonlinearity*, 17:1217-1244, 2004.
- [LT12] L.M. Lerman, D.V. Turaev. Breakdown of symmetry in reversible systems, *Regul. Chaotic Dyn.*, 17(3-4):318-336, 2012.
- [MR97] L. Mora, N. Romero. Moser's invariant curves and homoclinic bifurcations. *Dynam. Systems Appl.*, 6(1):29-41, 1997.
- [Rue81] D. Ruelle. Small random perturbations of dynamical systems and the definition of attractors. *Commun. Math. Phys.* 82:137151, 1981.
- [SV09] C. Simó, A. Vieiro. Resonant zones, inner and outer splitting in generic and low order resonances of area preserving maps. *Nonlinearity*, 22(5):1191-1245, 2009.
- [Tak74] F. Takens. Forced Oscillations and Bifurcations. *Applications of Global Analysis I. Communications of the Mathematical Institute Rijksuniversiteit Utrecht*, 3, 1974.